

In-depth comparison of Anc80L65 and AAV9 retinal targeting and characterization of cross-reactivity to multiple AAV serotypes in humans

Maura K. Schwartz,^{1,2} Shibi Likhite,¹ Tatyana A. Vetter,^{1,5} Megan C. Baird,^{1,2} Vicki McGovern,³ Andrea Sierra Delgado,¹ Tom Mendel,⁴ Arthur Burghes,³ and Kathrin C. Meyer^{1,2,5}

¹The Center for Gene Therapy, Nationwide Children's Hospital, Columbus, OH, USA; ²Biomedical Sciences Graduate Program, the Ohio State University, Columbus, OH, USA; ³Department of Neurology, the Ohio State University, Columbus, OH, USA; ⁴Department of Ophthalmology, the Ohio State University, Columbus, OH, USA; ⁵Department of Pediatrics, the Ohio State University, Columbus, OH, USA

Anc80L65 is a synthetic, ancestral adeno-associated virus that has high tropism toward retinal photoreceptors after subretinal injection in mice and non-human primates. We characterized, for the first time, the post-intravitreal cell-specific transduction profile of Anc80L65 compared with AAV9. Here we use Anc80L65 and AAV9 to intravitreally deliver a copy of the gene encoding GFP into WT C57Bl/6J mice. GFP expression was driven by one of two clinically relevant promoters, chicken β actin (CB) or truncated MECP2 (P546). After qualitative assessment of relative GFP expression, we found Anc80L65 and AAV9 to have similar transduction profiles. Through the development of a novel method for quantifying GFP-positive retinal cells, we found Anc80L65 to have higher tropism in Müller glia and AAV9 to have higher tropism in horizontal cells. In addition, we found P546 to promote GFP expression at a more moderate level compared with the high levels seen under the CB promoter. Finally, for the first time, we characterized Anc80L65 cross-reactivity in human sera; 83% of patients with AAV2 pre-existing antibodies were found to be seropositive for Anc80L65. This study demonstrates the expanded therapeutic applications of Anc80L65 to treat retinal disease and provides the first insights to Anc80L65 pre-existing immunity in humans.

INTRODUCTION

Adeno-associated viruses (AAVs) are naturally occurring, minimally immunogenic viruses that allow for sustained transgene expression, and hence have been developed into several successful gene replacement strategies.^{1–3} The retinal gene therapy field succeeded in obtaining the first approved AAV gene therapy, Luxturna, which utilizes a subretinal administration of AAV2 to target the retinal pigment epithelium (RPE) and deliver the RPE65 gene to patients with Leber congenital amaurosis.⁴ The second Food and Drug Administration (FDA)-approved AAV gene therapy, Zolgensma, followed shortly after with an intravenous administration of AAV9-SMN to treat spinal muscular atrophy (SMA) patients.^{5,6}

Several other retinal gene therapies are currently in development or in clinical trials, most of which use naturally occurring AAVs (serotypes

1–9) administered via the subretinal delivery route for treatment of retinal disorders affecting the photoreceptors or RPE.^{7,8} Despite their effectiveness, there are limitations to subretinal injections, including the risk of subretinal detachment.⁸ Furthermore, several studies have indicated that transgene expression is not achieved beyond the location of the subretinal bleb, the area where photoreceptors temporarily detach from the RPE as a consequence of subretinal injection.⁸ Finally, subretinal injections require the expertise of trained retinal surgeons and must be performed under anesthesia, thus increasing operative risk and cost.⁹ Intravitreal injection can overcome most of these limitations, however due to vitreous contact with the choroid, it leads to more exposure of the AAV to the intraocular immune system.^{9,10} As such, several pre-clinical and clinical studies have reported more adverse events related to intraocular inflammation after intravitreal injection.^{11–17} In addition, AAV vectors achieve limited transduction of photoreceptors after intravitreal injection due to the difficulties of penetrating the inner limiting membrane (ILM), which is a disadvantage of this approach for treatment of outer retinal diseases.^{16,18} For this reason, several strategies have been employed to overcome this physical barrier, including novel surgical techniques such as ILM peeling, among others.^{19–21} Unfortunately, these techniques introduce additional risk factors and potential complications. Therefore, the field has moved into the development of next-generation vectors.

Next-generation vectors involve capsid modification of naturally occurring AAVs via two primary methods. The first, termed rational design, makes intentional changes to the viral capsid based on previous knowledge of capsid structure, function, and how they influence tropism.²² The second, termed directed evolution, includes the selection of successful, random mutations typically followed by pre-clinical animal studies to identify functionality and novel tropic profiles.²³ Anc80L65

Received 30 September 2022; accepted 12 May 2023;
<https://doi.org/10.1016/j.omtm.2023.05.016>

Correspondence: Kathrin C. Meyer, PhD, The Center for Gene Therapy, The Research Institute, Nationwide Children's Hospital, 700 Children's Drive, Columbus, OH 43205, USA.

E-mail: kathrin.meyer@nationwidechildrens.org



(Anc80), developed via a form of rational design called ancestral sequence reconstruction, is gaining relevance within the retinal gene therapy field.^{24–26} Anc80 was identified through *in silico* phylogenetic reconstruction using a total of 75 sequences of AAV serotype isolates and variants and is predicted to be the ancestor of AAVs 1–3 and 6–9.²⁴ Previous studies have characterized the transduction of Anc80 in the retina after subretinal injection in both mice and non-human primates.^{24,25} These studies have shown Anc80 has higher affinity for the RPE and photoreceptors in mice when compared with AAV2 and AAV8 at a dose of 2E+09vg.²⁴ In non-human primates, higher tropism of the RPE and photoreceptor layers were observed after subretinal injection with Anc80L65 compared with AAV5 and AAV9.²⁵ To date, no previous studies have evaluated transduction of Anc80L65 after intravitreal injection. In addition, most biodistribution studies performed with Anc80L65 have utilized ubiquitous promoters.^{24,25,27} We hypothesized that Anc80 may be a suitable vector for intravitreal applications due to its relation to other serotypes successfully used for intravitreal injection, such as AAV2, AAV8, and AAV9.^{28–33}

In this study, we compared Anc80 and AAV9 transduction after subretinal and intravitreal delivery using a GFP reporter expression cassette. We used two clinically relevant ubiquitous promoters, the chicken β actin (CB) and truncated MeCP2 (P546) promoters. The P546 promoter is a short version of the MeCP2 promoter generated by the Kaspar lab. It allows expression of transgenes throughout the nervous system in multiple cell types such as astrocytes and neurons as well as peripheral organs. The promoter has proven efficacious in mice and is currently used in several AAV clinical trials.^{34,35} We have previously determined that P546 allows moderate, ubiquitous transgene expression after intracerebroventricular injection of AAV9 in wild-type (WT) C57/Bl6J mice compared with the strong expression profile seen with the CB promoter (Figure S1). However, this study is the first to evaluate the P546 promoter for expression pattern in the retina. We show that Anc80 and AAV9 have an overall similar transduction profile but with slightly different affinities for inner nuclear layer cells. In addition, we reaffirm that promoters can be used to modulate gene expression in specific subsets of cell types. Finally, because intravitreal injection risks greater exposure to the innate immune system and because Anc80 was previously shown to cross-react with AAV8, we investigated cross-reactivity of Anc80 with conventional serotypes AAV1, AAV2, AAV8, and AAV9 in human serum samples.^{9,24} We found that patients seropositive for AAV2 are more likely to be seropositive for Anc80 compared with AAV1, AAV8, or AAV9. This is a novel finding that suggests that immune profiles of next-generation vectors should be thoroughly investigated prior to translation to humans.

RESULTS

Subretinal delivery of AAV9 and Anc80L65 constructs in WT C57Bl/6J mice demonstrates efficient transduction of photoreceptors and RPE

To confirm the previously published reports of superior Anc80 outer retina transduction and evaluate differences in promoter-driven GFP expression, we subretinally injected C57Bl/6J mice with a total of four

vectors consisting of a GFP expression cassette driven by either the CMV enhancer chicken β -actin (CB) promoter or a truncated MeCP2 (546) promoter packaged in AAV9 or Anc80. The respective injected doses for each vector were as follows: AAV9.CB.GFP (2.03E+10vg), Anc80.CB.GFP (1.87E+10vg), AAV9.546.GFP (1.96E+10vg), and Anc80.546.GFP (1.28E+10vg). Vector concentration was determined using transgene-specific digital droplet PCR (Table S1). While three vectors had very similar concentrations and differences were within assay variability range, the fourth one (Anc80.546.GFP) had a lower concentration. Thus, due to differences in concentration and the volume restriction for intraocular injections, we could not inject the exact same dose for all vectors. All results were evaluated with this distinction in mind. WT C57Bl/6J mice were injected at 2–4 months of age and were killed 4–8 weeks post-injection. During this period, we expect to reach peak GFP expression without any loss of signal, allowing direct comparison of efficacy.

After immunofluorescent staining of retinal cryosections with anti-GFP and anti-recoverin, we observed comparable transduction and GFP signal in the RPE and photoreceptors with AAV9.CB.GFP and Anc80.CB.GFP vectors (Figures 1B and 1C). However, compared with AAV9.546.GFP-injected eyes, GFP signals were higher in photoreceptors and the RPE in Anc80.546.GFP-injected eyes as observed by increased GFP co-localization with recoverin (photoreceptors/RPE) counterstain (Figures 1B and 1C). This was despite the Anc80.546 dose being lower compared with AAV9.546.GFP. Thus, these results confirm the previous reports of high RPE and photoreceptor tropism of Anc80 following subretinal administration. In general, we observed higher GFP expression levels in our CB constructs compared with our P546 constructs (Figures 1B and 1C), which is in line with the P546 promoter leading to a more moderate expression level compared with the CB promoter. Finally, spread of GFP expression beyond the injection site was observed in both AAV9- and Anc80-injected eyes (Figure 1A).

Intravitreal delivery of AAV9 and Anc80L65 in WT C57Bl/6J results in unique transduction profiles but comparable retinal cell-type tropisms

Similar to subretinal injections, 2- to 4-month-old WT C57Bl/6J mice were intravitreally injected with AAV9.CB.GFP (2.03E+10vg), Anc80.CB.GFP (1.87E+10vg), AAV9.546.GFP (1.96E+10vg), and Anc80.546.GFP (1.28E+10vg) in 2 μ L. Four to 8 weeks post-injection, a period in which peak transgene expression is reached and no loss of expression is expected, we qualitatively assessed retinal transduction within cell types of interest via immunofluorescent staining on retinal cryosections. Samples were labeled with anti-GFP antibody and counterstained with several cell-type-specific antibodies: anti-Brn3a (ganglion), anti-AP-2 α (amacrine), anti-Sox2 (Müller glia), anti-Otx2 (bipolar), and anti-Calb (horizontal). z stack images were obtained on a Zeiss 800 Laser Scanning Confocal Microscope and maximum intensity projections acquired with orthogonal views. Transduction and perceived cell-type-specific promoter-driven expression was assessed individually for each vector and is based on qualitative assessments, including the degree of co-localization between GFP and

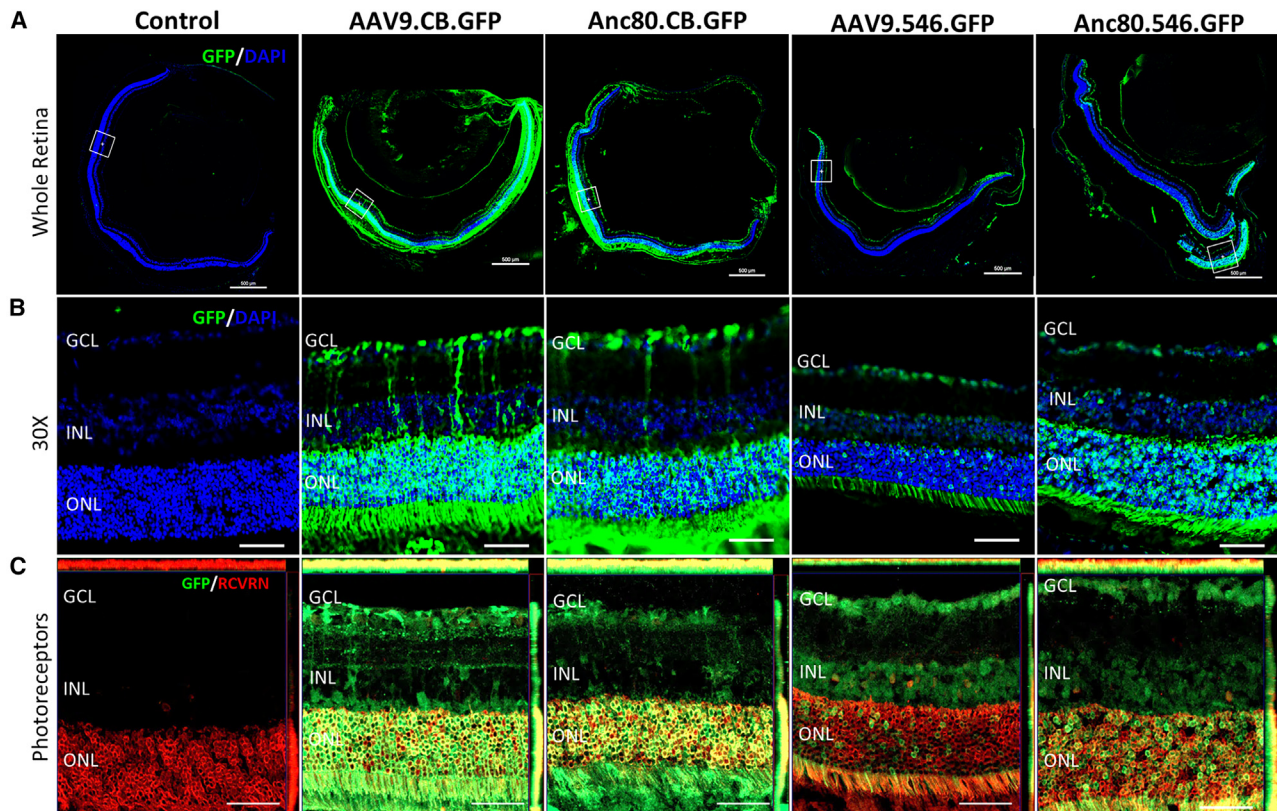


Figure 1. Anc80 vector has increased tropism for photoreceptors and RPE compared with AAV9 after subretinal injection in WT C57Bl/6J mice

Representative immunofluorescent images of retinas comparing AAV9.CB.GFP ($n = 4$), Anc80.CB.GFP ($n = 3$), AAV9.546.GFP ($n = 3$), and Anc80.546.GFP ($n = 3$) transduction after subretinal injection. (A) Large-Scan 30X stitched image of whole retina taken on Nikon Ti-2E Inverted Microscope. GFP is shown with DAPI overlay; $\times 20$ objective with 1.5 magnification; scale bar, 500 μm . (B) A 30X single region of interest originating from white boxes in images in (A); $\times 20$ objective with 1.5 magnification; scale bar, 50 μm . (C) z stack maximum intensity projection images with orthogonal views taken on Zeiss 800 LSM Confocal with $\times 20/0.8$ M27 objective and 1.5 digital zoom. Representative images show GFP (green) expression with RCVRN⁺ photoreceptors in red. Scale bar, 50 μm . GCL, ganglion cell layer; GFP, green fluorescent protein; INL, inner nuclear layer; ONL, outer nuclear layer; RCVRN, recoverin.

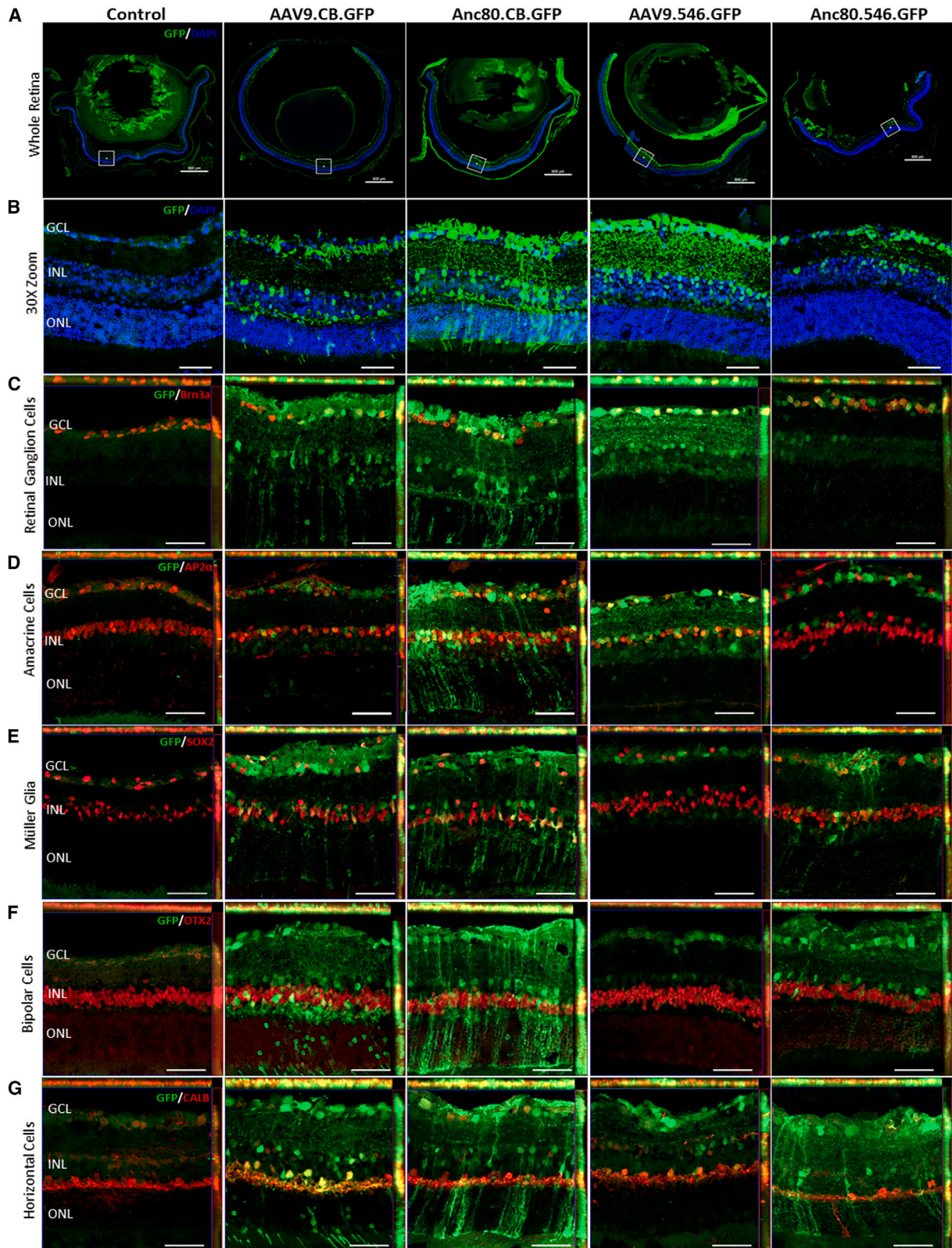
cell-type markers, and the relative fluorescent intensity observed in orthogonal views.

Figure 2A shows whole retina along with $\times 30$ zoom insets (Figure 2B) taken at specific regions of interest. Each serotype displays its own unique transduction pattern (Figure 2B). AAV9.CB.GFP demonstrates the highest transduction within ganglion cells and horizontal cells, based on significant co-localization among GFP, Brn3a, and Calb (Figures 2C and 2G). Comparatively, less co-localization of GFP was observed in AP-2 α -, Sox2-, and Otx2-positive cells, indicating moderate transduction of amacrine cells, Müller glia, and bipolar cells, respectively (Figures 2D–2F). Orthogonal views indicate higher levels of co-localization within bipolar cells, but we predict this may be confounded by the overlap of GFP-positive horizontal cells.

Anc80.CB.GFP administration results in high transduction of ganglion cells and Müller glia, indicated by high levels of GFP co-localization with Brn3a and Sox2, respectively (Figures 2C and 2E).

Moderate transduction of amacrine and bipolar cells was observed, as indicated by positive overlap among GFP, AP-2 α , and Otx2, respectively (Figure 2D). Finally, less co-localization between GFP- and Calb-positive cells was observed, indicating lower transduction rates among horizontal cells (Figures 2F and 2G). Orthogonal views suggest high levels of co-localization within bipolar cells, but we predict this may be confounded by the overlap of GFP-positive Müller glia processes (Figure 2F).

A similar level of co-localization, compared with AAV9.CB.GFP retinas, was seen in ganglion cells, amacrine cells, and horizontal cells after AAV9.546.GFP intravitreal administration, as indicated by positive GFP expression within Brn3a-, AP-2 α -, and Calb-labeled cells, respectively (Figures 2C, 2D, and 2G). Co-localization between GFP and Sox2 or Otx2 was not observed (Figures 2E and 2F). After Anc80.546.GFP administration, co-localization of GFP with most cell types was low to moderate except for in Brn3a positive ganglion cells, which was comparatively higher (Figure 2C). Orthogonal views again suggest co-localization of GFP with Otx2 (bipolar), and Calb



(legend on next page)

(horizontal), but we again predict this to be partially confounded by the positively transduced Müller glia processes (Figures 2F and 2G).

Automated AI-based image analysis allows for efficient retinal cell quantification

A custom analysis workflow was developed in a blinded fashion on the Nikon NIS-Elements software platform to automatically detect individual retinal cells using the SegmentObjects.ai convolutional neural network module, and to identify GFP-positive cells using an empirically calculated GFP threshold without any operator input to avoid bias (Figure 3A). After confirming the accuracy of the novel Nikon AI-based retinal cell quantification method by comparing it with previously obtained hand counts (Figure S2), we used it to quantify the number of GFP-positive cells of each retinal cell type (Figures 3B and 3C). This allowed us to increase the validity and rigor of our co-localization visualizations performed in Figure 2.

Overall, the retinal cell GFP quantification aligned well with initial qualitative assessments. AAV9.CB.GFP (Figure 3D) transduced almost 50% of ganglion and horizontal cells and 20% of amacrine cells. This was followed by only about 13% transduction within Müller glia and bipolar cells, which were transduced at statistically significantly lower rates. Anc80.CB.GFP (Figure 3E) transduced ganglion cells and Müller glia most efficiently with 31% and 23% of cells targeted, respectively. Transduction rate in amacrine cells was 18%, followed by 15% and 9% in bipolar and horizontal cells, respectively. Significant differences were only observed between average transduction rates of ganglion cells and horizontal cells. AAV9.546.GFP (Figure 3F) maintained high GFP expression within ganglion and horizontal cells with counts revealing 50% and 34% positivity, respectively. The average number of GFP-positive ganglion and horizontal cells was significantly higher compared with GFP-positive amacrine (15%), Müller glia (2%), and bipolar cells (4%). Finally, Anc80.546.GFP (Figure 3G) administration resulted in significantly higher numbers of GFP-positive ganglion cells (41%) compared with all other cell types. The percentage of GFP-positive amacrine, Müller glia, bipolar, and horizontal cells were all below 10%. The lower rate of co-localization in Anc80.546.GFP retinas is most likely due to the lower dose that was delivered at time of injection. Finally, we quantified relative GFP expression within photoreceptors, as described in detail in the methods. We found that all vectors in this study achieved relatively low transduction levels of less than 5% following intravitreal injection (Figure S3). Anc80.CB.GFP seemingly achieved the highest transduction of pho-

photoreceptors at around 4%, although this could be a slight overestimation due to some overlap of Müller glia processes with the nuclei of photoreceptor cells.

Since AAV9.CB.GFP, Anc80.CB.GFP, and AAV9.546.GFP were administered at similar doses, we performed additional analysis comparing the respective vector transduction rates within each individual cell type. One-way ANOVA with Tukey's multiple comparisons test was performed between all groups and pairwise comparisons graphed between AAV9.CB.GFP and AAV9.546.GFP and between AAV9.CB.GFP and Anc80.CB.GFP (Figure S2). In comparing AAV9.CB.GFP with AAV9.546.GFP, significant differences were found in average GFP co-localization within bipolar cells and Müller glia. In addition, the percentage of GFP-positive cells was generally lower in all cell types of AAV9.546.GFP-treated eyes. When comparing Anc80.CB.GFP with AAV9.CB.GFP, transduction was significantly increased in Müller glia and significantly decreased in horizontal cells. Relative transduction in ganglion, amacrine, and bipolar cells was similar.

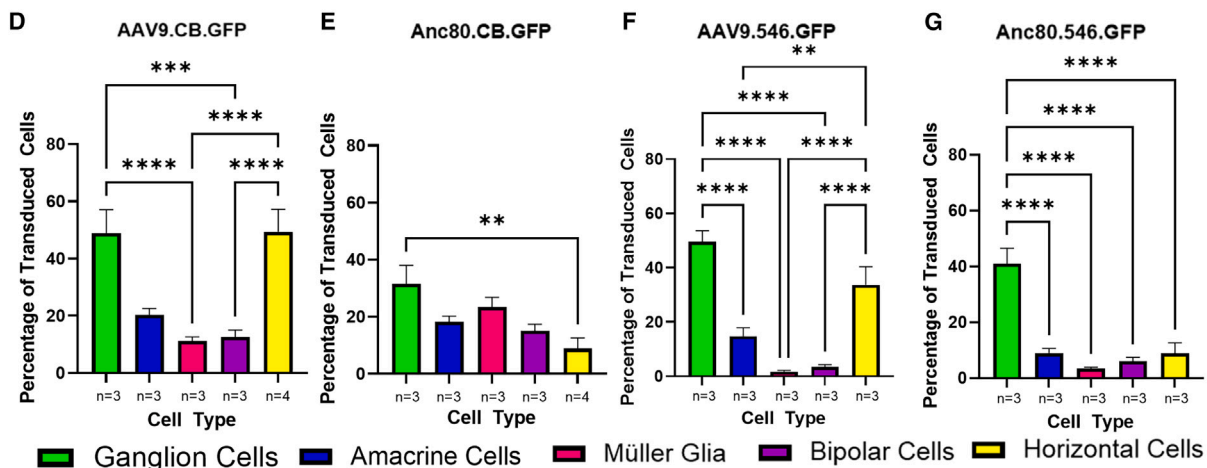
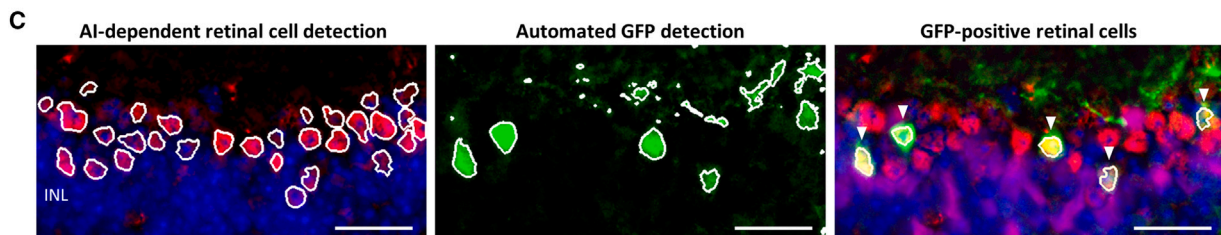
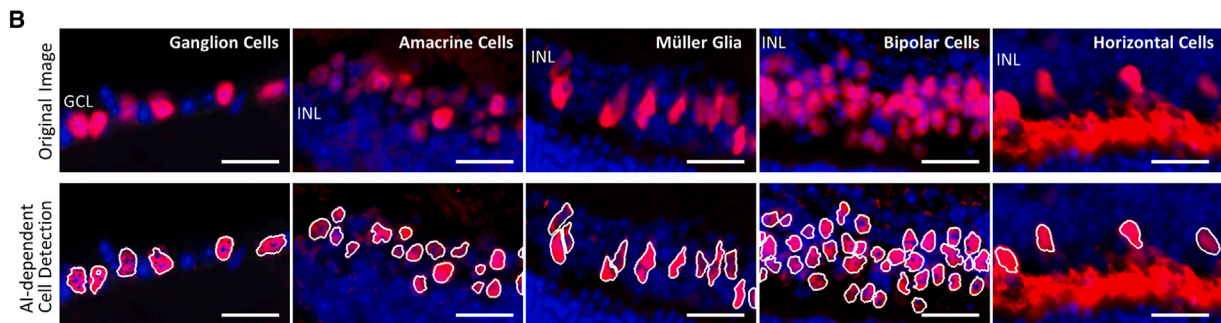
Human samples with high AAV2 pre-existing antibodies have higher pre-existing immunity toward Anc80 than other naturally occurring AAV serotypes

Anc80 capsids are not naturally occurring, rather, they were developed by capsid evolution processes in search for common ancestral AAV motifs. Therefore, it is important to determine whether antibodies against naturally occurring and closely related capsids induce an immune response to Anc80. To evaluate whether pre-existing antibodies for AAV1, AAV2, AAV8, and AAV9 might be cross-reactive to Anc80, we screened 12 human serum samples using antibody-binding enzyme-linked immunosorbent assay (ELISA). The samples used in this study are from human subjects that had not received AAV-related therapies prior to serum collection. Each well of the ELISA plate was coated with $1E+9$ vector particles for each capsid. Serial dilutions of the serum began at 1:50 and ended at 1:3,200 for the initial pre-screen. Samples that were positive at 1:3,200 were tested again on an additional ELISA assay with serial dilutions beginning at 1:800 and ending at 1:102,400 to determine the endpoint titer. Samples that read positive at and above 1:50 serum dilution were considered seropositive.

Of the 12 samples tested, 11 were seropositive for AAV2. Surprisingly, of those 11 AAV2-positive samples, 10 of them were also seropositive for Anc80. Of the samples that were AAV2 and Anc80 positive, eight

Figure 2. Anc80 and AAV9 vectors primarily transduce ganglion cells and display different inner nuclear layer tropisms after intravitreal injection in WT C57Bl/6J mice

Representative immunofluorescent images of retinas comparing AAV9.CB.GFP (n = 4), Anc80.CB.GFP (n = 3), AAV9.546.GFP (n = 3), and Anc80.546 (n = 3) transduction after intravitreal injection. (A) Large-scan 30X stitched image of whole retina taken on Nikon Ti-2E Inverted Microscope. GFP is shown with DAPI overlay; $\times 20$ objective with 1.5 magnification; scale bar, 500 μm . (B) A 30X single region of interest originating from white boxes in images in (A); $\times 20$ objective with 1.5 magnification; scale bar, 50 μm . (C–G) z stack maximum intensity projection images with orthogonal views taken on Zeiss 800 LSM Confocal microscope with $\times 20/0.8$ M27 objective and 1.5 digital zoom; scale bar, 50 μm . Double immunolabeling of GFP in green with Brn3a⁺ ganglion cells (C), AP-2 α ⁺ amacrine cells (D), Sox2⁺ Müller glia (E), Otx2⁺ bipolar cells (F), and Calb⁺ horizontal cells (G) in red. Representative images for each counterstain within the same treatment group originate from different sections of the same eye or from multiple mice and demonstrate heterogeneous transduction. Calb, calbindin; GCL, ganglion cell layer; GFP, green fluorescent protein; INL, inner nuclear layer; ONL, outer nuclear layer.



H AAV serotype and promoter dependent cell type expression matrix

Serotype	Promoter	Ganglion	Amacrine	Müller Glia	Bipolar	Horizontal
AAV9	CB	+++++	+++	++	++	+++++
Anc80	CB	++++	+++	+++	++	+
AAV9	546	+++++	++	-	-	++++
Anc80	546	+++++	+	-	+	+

Above 40% = +++++; Above 30% = ++++; Above 20% = +++; Above 10% = ++; Above 5% = +; Below 5% = -

(legend on next page)

were simultaneously seropositive for AAV1, AAV8, and AAV9. Thus, eight samples were positive for all serotypes included in the assay. Only one sample screened was determined to be seronegative for all capsids. These results are summarized in Figure 4B. Not only were samples that were AAV2 positive more likely to be Anc80 positive, they also generally had higher antibody-binding titers for Anc80 compared with the other screened capsids (Figure 4). As anti-AAV2 binding titers decrease, other anti-AAV binding titers decrease as well. Of the eight samples that were seropositive for all capsids, seven of them had anti-Anc80 antibody titers that were higher than anti-AAV1, anti-AAV8, and anti-AAV9 binding titers. Only two samples were more seropositive for AAV9 than Anc80.

DISCUSSION

In recent years, the AAV gene therapy field has made significant strides in developing next-generation vectors that aim to overcome limitations of current, conventional vectors, mainly by engineering new variants or rationally modifying natural variants to increase specificity for certain tissues and cell types.^{36–38} An additional goal of these variants is to evade recognition by pre-existing antibodies within the general population.³⁹ Anc80L65 is a next-generation vector that was *in silico* designed based on ancestral sequence reconstruction.²⁴ It was designed to maintain the structural and functional attributes of conventional AAVs, but with an attempt to also be immunologically distinct from them.²⁷ Many studies in recent years have demonstrated that Anc80 is a potent gene therapy vector with applications in retinal, cochlear, and liver disorders.^{40–44} AAV9 and close relatives are also commonly used candidate vectors for the development of new gene replacement therapies due to their proven efficacy, established manufacturing methods, and their known success in the clinic.^{6,33–35,45,46}

As previously mentioned, one study had found that Anc80 has a higher transduction efficiency, compared with AAV9 after subretinal injection, within cone photoreceptors and the RPE in both mice and NHPs.⁴⁷ This previous study utilized single-stranded vector constructs with the CMV promoter. In our study, we wanted to compare the transduction efficiency of AAV9 and Anc80 with constructs containing self-complementary packaged genomes and two clinically relevant promoters. Although self-complementary genomes reduce AAV vector packaging capacity by half, they can reduce time to expression, which might be critical to prevent ongoing retinal degeneration and halt progressive vision loss.⁴⁸ In addition, the choice of capsid is an important consideration with respect to the ability of the vector to cross the ILM to allow for efficient transduction. Last,

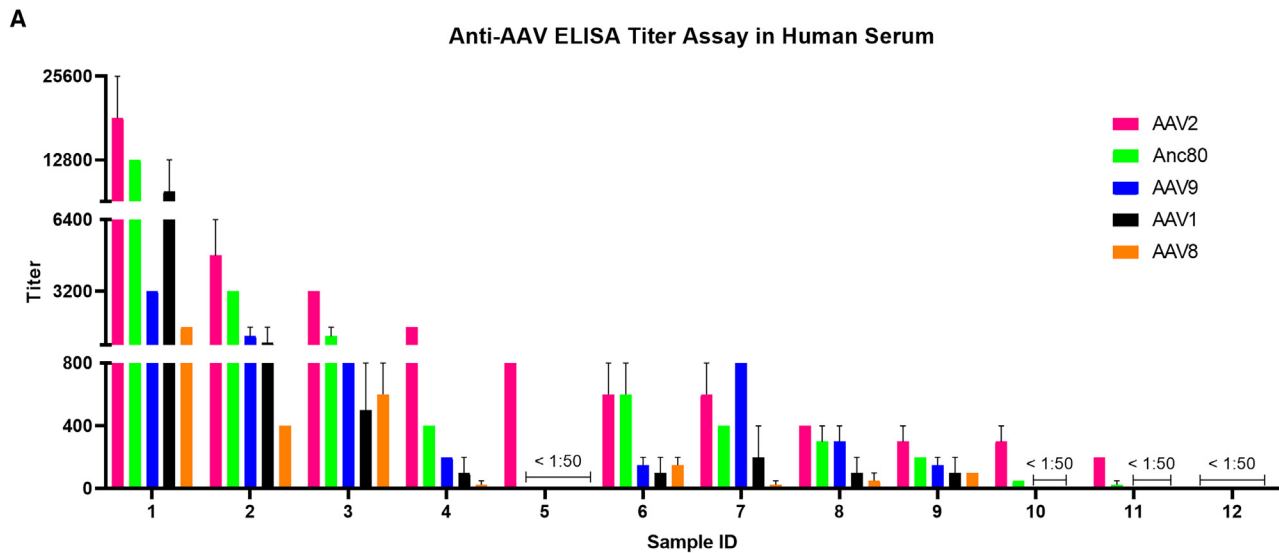
the transgene expression level or pattern can be strongly influenced by the promoter. The chicken beta-actin (CB) promoter stimulates ubiquitous transgene expression and is currently used in the FDA-approved SMA gene replacement strategy (Zolgensma) and in other clinical therapies, such as CLN6 gene replacement for Batten Disease.^{6,46} The truncated MeCP2 (P546) promoter was developed in the Kaspar lab and also allows ubiquitous expression but at a more moderate level. The expression pattern of the P546 promoter in the retina has not been evaluated to date.

After subretinal injection in WT C57Bl/6J mice, AAV9.CB.GFP and Anc80.CB.GFP yielded similar transduction efficiencies for the photoreceptor layer and the RPE. In contrast, Anc80.546.GFP achieved higher GFP expression in the outer nuclear layer (ONL) compared with AAV9.546.GFP despite being administered at a lower dose. Taken together, these results confirm previously published reports of Anc80's superior photoreceptor tropism. Since the CB promoter yields a stronger expression level compared with the P546 promoter, it might be more difficult to spot differences in transduction patterns at higher doses. The use of lower expressing promoters could be beneficial, as a recent study by Xiong et al. discovered that the use of strong ubiquitous promoters in AAV constructs led to ocular toxicity after subretinal injection in mice.⁴⁹ Therefore, the usage of moderate promoters such as the P546 might be an attractive strategy to avoid overexpression issues. However, following histological analysis of the retinas included in this study, toxicity was not observed with either CB or 546 vector constructs (Figure S5). Both ONL and inner nuclear layer (INL) thickness were well preserved compared with the uninjected control group and no significant pathology was observed.

While the majority of vision disorders stem from photoreceptor dysfunction, many also involve cell types of the inner retina such as ganglion cells and bipolar cells. Such diseases include glaucoma, hereditary optic neuropathies, congenital stationary night blindness, and Batten disease, among others.^{50–53} In addition, almost all retinal diseases are associated with reactive Müller glia and inflammation. While Müller glia are the most abundant glia in the retina and are typically protective of neurons, disease-related gliosis in some cases will support survival of neurons and in others can further accelerate retinal degeneration.^{54,55} Because vectors delivered subretinally only efficiently transduce the ONL, intravitreal injections must be used to reach cells of the inner retina. In the context of AAV gene therapy, the ILM, a physical barrier between the vitreous and retina, is known to limit successful transduction.^{18,56} Nonetheless, previous studies

Figure 3. NIS-Elements AI analysis enables accurate, non-biased quantification of individual retina cell-type transduction

(A) Overview of automated GFP expression analysis approach. Steps outlined in black were completed manually by an operator, and steps shown in gray were performed identically and automatically in batches without operator input. (B) Representative images of final neuron detection (white outlines) for each analyzed cell type. Scale bar, 20 μ m. (C) Representative images of GFP-positive neuron identification based on automated GFP signal detection and AI-based neuron selection. Scale bar, 20 μ m. (D–G) Retina counts, graphed separately per vector (AAV9.CB.GFP, Anc80.CB.GFP, AAV9.546.GFP, and Anc80.546.GFP), correspond with IHC data in Figure 2. N = # below graphs indicate number of eyes sampled. At least three sections per eye were included in quantification to account for previously observed heterogeneous transduction. Ordinary one-way ANOVA analysis was performed between the average percent of transduction within each retinal cell type. *p < 0.05; **p < 0.01; ***p < 0.001. (H) Relative transduction efficiencies, based on cell counts, are shown in an expression matrix. See also Figures S2 and S4.



B

Summary of average anti-AAV ELISA binding titers

Sample ID	AAV2	Anc80	AAV9	AAV1	AAV8
1	1:19200	1:12800	1:3200	1:8000	1:1600
2	1:4800	1:3200	1:1200	1:900	1:400
3	1:3200	1:700	1:800	1:500	1:600
4	1:1600	1:400	1:200	1:100	1:25
5	1:800	<1:50	<1:50	<1:50	<1:50
6	1:600	1:600	1:150	1:100	1:150
7	1:600	1:400	1:800	1:200	1:25
8	1:400	1:300	1:300	1:100	1:50
9	1:300	1:200	1:150	1:100	1:100
10	1:300	1:50	<1:50	<1:50	<1:50
11	1:200	1:25	<1:50	<1:50	<1:50
12	<1:50	<1:50	<1:50	<1:50	<1:50

Figure 4. AAV2 binding antibody titers correlate with Anc80 binding antibody titers

Twelve human serum samples were screened to determine AAV1, AAV2, AAV8, AAV9, and Anc80 antibody-binding titers via ELISA assay in duplicate. (A) Samples are graphed from highest to lowest AAV2 antibody titers. Bracket symbols on the graph indicate values that fell below the cutoff of 1:50 in this assay. (B) Averaged anti-AAV binding titers per serotype are listed.

have reported successful AAV9 transduction in ganglion cells, amacrine cells, Müller glia, and horizontal cells after intravitreal injection in mice.^{32,57} Efficacy of intravitreal AAV9 was additionally proven by the success of gene replacement in CLN5 Batten Disease sheep, which was recently translated to a clinical trial.³³ To date there have been no studies published regarding the transduction profile of Anc80 after

intravitreal injection. We sought to compare AAV9 and Anc80 targeting after intravitreal injection to evaluate whether Anc80 would lead to a superior transduction pattern using this injection route as well. Using the same experimental approach as our subretinal studies, we found Anc80 and AAV9 to have similar transduction profiles overall but interestingly found slightly different expression patterns

in INL cell types. We were able to characterize the transduction efficiency of each serotype within each major cell type with the development of a novel, artificial intelligence program that permits non-biased and accurate quantification of positively transduced retinal cells. This program could easily be adapted for other applications, such as quantifying retinal cell loss in disease models.

Both Anc80 and AAV9 had high and moderate transduction efficiency within ganglion cells and amacrine cells, respectively, and low transduction rates with bipolar cells and photoreceptors after intravitreal delivery. AAV9 was able to transduce horizontal cells significantly better than Anc80, while Anc80 was able to transduce Müller glia significantly better than AAV9. These differences in transduction, along with slight variations in promoted transgene expression between promoters CB and P546, suggest that each capsid and promoter combination could have its own specific applications. Drawing from Figure 3H, AAV9 and Anc80 vectors with CB promoter constructs will allow for high transgene expression in several cell types after intravitreal injection and may be beneficial for retinal diseases that stem from the absence of a secreted protein. Indeed, it is predicted that the success of AAV9.CBh.CLN5 treatment in sheep, now translated to clinic (NCT05228145) as a dual intracerebroventricular and intravitreal administration approach, benefited from cross-correction whereby functional protein was secreted from successfully transduced cells.³³ Like CLN5 Batten Disease, several other secondary retinal disorders such as Mucopolysaccharidosis I, Refsum disease, and other forms of Batten Disease, may benefit from a similar combined treatment approach whereby Anc80 or AAV9 could be delivered to both brain and eye to combat CNS and retinal pathologies.^{58,59} Last, we found the P546 promoter allows for moderate expression in ganglion and horizontal cells and might be a more desirable choice to avoid overexpression toxicity in other cell types. Both cell types are highly desirable targets within the optogenetic gene therapy field.⁶⁰

Finally, we characterized the cross-reactivity between Anc80 and its direct, conventional AAV descendants in the context of human immunology for the first time. Previous studies indicate low cross-reactivity of Anc80 to other AAV serotypes.²⁴ Zinn et al. used rabbit sera raised against conventional serotypes 1, 2, 5, 6.2, 8, 9, rh32.33, and rh.10 to test their ability to neutralize Anc80.²⁴ Results indicated low-level cross-reactivity with AAV2 and AAV8, but not AAV9 or rh.10.²⁴ Partial cross-reactivity between AAV8 and Anc80 was also demonstrated *in vivo* in mice.²⁴ Surprisingly, there was no cross-reactivity between Anc80 and rh.10 even though they only differ by 8.6% of residues.²⁴ AAVrh10 is a recombinant vector isolated from rhesus macaque and previous studies report that 59% of a screened healthy population had immunoglobulin (Ig)G prevalence against AAVrh10.⁶¹ The same study reported AAV2 and AAV9 IgG prevalence to be 72% and 47%, respectively.⁶¹ Given these previous findings, we wanted to investigate the seroprevalence and cross-recognition of Anc80 in human serum. Human serum studies are valuable, as previous reports have published evidence that serum antibody titers can effectively neutralize AAV and prompt intraocular inflammation after intravi-

treteal injection.^{62,63} While the eye is considered an immune privileged site, it is not absolute.⁶⁴ The risk of inflammation is higher after intravitreal injection, but can also occur after subretinal injection.⁶⁵ Notably, Anc80.CMV.GFP delivered subretinally in dogs with retinitis pigmentosa resulted in severe inflammation that corresponded with reduced efficacy.⁶⁵ However, it was not determined if this was due to effects from the expression cassette or the capsid itself.⁶⁵

Our study found that human individuals who have pre-existing immunity against AAV2 might also have immunity against Anc80. Out of the 12 samples screened, 83% were Anc80 positive compared with 67% that were AAV9 positive. All samples that were Anc80 and AAV9 positive were also AAV2 positive. Overall, these preliminary results suggest that Anc80 may not be as immunologically distinct as initially thought. Further efforts are being made to expand the sample size of the current study. In addition, more studies are required to assess the extent of neutralization by these sera. Neutralizing antibodies are known to reduce transduction of AAV vectors via immune activation and therefore can affect the efficacy of gene therapy treatments.⁶⁶ Nonetheless, immune activation can still be triggered by non-neutralizing antibodies and lead to inflammation and other adverse events in humans.⁶⁶

Overall, our study provides in-depth characterization of the cell-type-specific tropisms of AAV9 and Anc80 within the rodent retina following traditional intraocular routes. These data can be used to inform future clinical applications. However, additional studies are needed to evaluate the transduction profiles of these vectors in the context of larger animal models. It is well known that capsid tropism can change between species. In addition, there are key differences in ocular characteristics between rodents and larger mammals, such as ILM composition and vitreous humor volume, which are known to limit AAV diffusion and transduction.^{18,19,67,68} Last, we show that there may be higher risk of pre-existing immunity in humans toward Anc80 than previously predicted. Further studies are required to better elucidate the potential risks of future Anc80 gene therapy strategies in clinic.

MATERIALS AND METHODS

Animals

All procedures were performed in accordance with the NIH Guidelines and approved by the Abigail Wexner Research Institute at Nationwide Children's Hospital (Columbus, OH). C57BL6J mice were obtained from Jackson Laboratories (Bar Harbor, ME). The mice were group housed under a 12-h light-dark cycle with *ad libitum* access to food and water. Both male and female mice were included in the transduction analyses.

Vectors

A GFP reporter transgene was cloned into an AAV transfer plasmid under the control of the chicken β actin (CB) or truncated *MecP2* (P546) promoter. Transfer plasmids were then packaged into AAV9 or Anc80L65 constructs. We thank Luk H. Vandenberghe for contributing the Anc80L65 plasmid. Self-complementary AAV9 vectors were produced by transient transfection procedures using a

Table 1. Droplet digital PCR primers and probes

GFP forward primer (900 nM)	5'CCACTACCTGAGCACCCAGTC
GFP reverse primer (900 nM)	5'TCCAGCAGGACCATGTGATC
GFP probe (250 nM)	FAM-TGAGCAAAGACCCCAACGAGAAGCG

nM, nano-molar.

double-stranded AAV2-ITR-based vector, with a plasmid encoding Rep2Cap9 sequence as previously described along with an adenoviral helper plasmid pHelper (Stratagene, Santa Clara, CA) in 293 cells. AAV9.CB.GFP has been described previously.^{69,70} Silver staining analysis was originally used to measure the purity and titer of the vector.

AAV titration by droplet digital PCR

Titration of different AAV vectors was performed by droplet digital PCR (ddPCR) as previously described.⁷¹ Briefly, purified vectors were diluted 10-fold and treated with DNase I (Roche Applied Science, Indianapolis, IN) at 400 U/mL for 30 min at 37°C. Treated samples were then diluted to within the detectable range of ddPCR using the dilution buffer (1x PCR buffer [Applied Biosystems, Foster City, CA], 2-ng/μL sheared salmon sperm DNA [Invitrogen, Carlsbad, CA], and 0.05% Pluronic F-68 [Invitrogen]). The reaction mixtures were assembled with the recommended ddPCR supermix (Bio-Rad, Hercules, CA), appropriate primers and probes (Table 1), and template (5 μL) in a final volume of 20 μL. Droplets were generated, then transferred to a 96-well PCR plate and amplified to the endpoint (50 cycles) with a conventional thermal cycler. The PCR reactions were read on a QX200 droplet reader (Bio-Rad), and the data were analyzed with QX Manager software (Bio-Rad). The viral titer was calculated as previously described.⁷¹ See also Table S1.

Subretinal injection

Two-month-old mice were anesthetized with ketamine/xylazine cocktail and total administration volume (2 μL) loaded into pulled glass borosilicate needles (100 μm). Vectors were diluted with phosphate buffered saline, if needed. Proparacaine hydrochloride ophthalmic solution (0.5%) and Tropicamide ophthalmic solution (0.5%) were applied generously for anesthetic and to dilate the eyes, respectively. Eyes were protruded and kept in place by a single, temporary surgical suture. A 30-G needle (BD Precision Glide, Franklin Lakes, NJ, CAT305106) was used to puncture the posterior sclera followed by insertion of the pre-filled glass needle and vector administration. Antibiotic ointment and lubricant were applied after injection to prevent infection and corneal ulceration. Three eyes were injected per vector, with the exception of AAV9.CB.GFP where four eyes were injected. Animals were killed at least 4 weeks post-injection for eye processing.

Intravitreal injection

Pre- and post-injection procedures were performed as described for subretinal injections. Administration volume (2 μL) was loaded into a 5-μL Hamilton syringe with 30-G needle. A separate 30-G needle (BD Precision Glide, CAT305106) was used to puncture the dorsal

sclera of 2-month-old mice followed by administration of vector into the vitreous chamber. Three eyes were injected per vector, with the exception of AAV9.CB.GFP where four eyes were injected. Animals were killed at least 4 weeks post-injection for eye processing.

Eye processing

At 4 weeks post-injection mice were killed by ketamine/xylazine overdose followed immediately by cardiac saline perfusion. For immunohistochemistry, eye globes were extracted and placed in 4% paraformaldehyde for 2 h. Eyes were briefly washed in PBS before transfer to sucrose gradient. Eyes were placed in 5% sucrose for 30 min, 10% sucrose for 30 min, and 20% sucrose overnight. Eyes were embedded in OCT, cut on a cryostat into 14-μm cross-sections, and placed onto Superfrost microscope slides (Fisher Scientific, Waltham, MA).

Immunohistochemistry

Briefly, on-slide retina sections were surrounded by a hydrophobic barrier (Vector Labs ImmEDGE hydrophobic barrier pen, Newark, CA) and washed three times for 10 min in Tris-buffered saline (TBS). Permeabilization and blocking steps were not performed prior to primary antibody incubation overnight at room temperature. Primary antibodies were diluted in TBS buffer containing 0.2% Triton-100. Antibodies used were as follows: Rabbit anti-Brn3a (ab245230 [1:100]; Abcam, Cambridge, UK), Mouse anti-AP-2 alpha (3B5 [Undiluted], Developmental Studies Hybridoma Bank, University of Iowa, Iowa City, IA), Goat anti-Sox2 (AF2018 [1:1000], R&D Systems, Minneapolis, MN), Goat anti-Otx2 (AF1979 [1:1000], R&D Systems), Mouse anti-Calbindin (MCA-4H7 [1:500], Encor Biotechnology, Gainesville, FL), Rabbit anti-Recoverin (AB5585 [1:1000], Millipore Sigma, Burlington, MA), Chicken anti-GFP (1:400, Abcam, ab13970). Slides were washed three times in TBS for 10 min. Sections were incubated for 1 h at room temperature in the appropriate fluorescein isothiocyanate-, GFP-, Cy3-, or Cy5-conjugated secondary antibodies (Jackson ImmunoResearch, Westgrove, PA), and DAPI (Invitrogen). Slides were washed three times in TBS for 10 min then followed by 3- to 4-min incubation with True Black Lipofuscin Autofluorescence Quencher (23007, Biotium, Fremont, CA). Slides were washed two times in TBS for 5 min then coverslipped with ProLong Gold Antifade Mountant (CatP36930, Thermo Fisher Scientific, Waltham, MA). Images were captured on a Nikon Ti2E inverted fluorescent microscope or Zeiss LSM 800 confocal microscope.

AI-based retinal cell quantification

Data were sampled from at least n = 3 eyes per vector construct. Five retina cryosections were obtained from each eye and used for on-slide IHC. The first section of each slide was used as a secondary only antibody control to assess nonspecific antibody binding. For analysis, a 30X single image was captured from a single region of interest from three of the four remaining sections.

Analysis was performed on original multichannel 16-bit images in Nikon NIS-Elements AR software (version 5.41) with the General Analysis 3 (GA3) and NIS.ai software modules. All processing and

analysis steps were completed automatically on all images in batches except where stated otherwise. The analysis workflow and custom GA3 quantification algorithms were developed and optimized by an unbiased third-party operator while blinded to the treatment groups (Figure 3A).

Images were processed in GA3 with denoising, 2D deconvolution, and subtraction of valleys from peaks to enhance features in the retinal cell marker channel. A SegmentObjects.ai module, trained for 1,000 iterations on images of 793 manually segmented retinal cells to a training loss of 0.0113, was then used for automated detection of individual retinal cells in these processed images. The main retinal layer containing each detected cell type was automatically outlined to restrict subsequent analysis steps to the appropriate region. Following the AI-dependent retinal cell detection process, an operator inspected images for errors and made manual corrections to the detected retinal cell and layer binary regions as needed to finalize the retinal cell segmentation (Figure 3B).

After manual operator corrections, GFP expression was automatically analyzed in all images in a second batch GA3 process without any operator input to eliminate bias. The GFP channel of each image was processed with rolling ball background subtraction (8- μ m radius) to reduce background, and an auto-threshold calculated from the nonspecific GFP signal at the appropriate retinal layer in each image was used to define GFP-positive pixels. Each identified retinal cell was then determined to be GFP-positive or GFP-negative based on any overlap of its centroid with GFP-positive signal (Figure 3C), and a set of binary image layers and numerical values representing the results was exported for each image.

Photoreceptor layer GFP quantification

Using the GA3 module in NIS-Elements, 16-bit multichannel images were processed with 2D deconvolution in the DAPI channel and rolling ball background subtraction in both the DAPI and GFP channels. Bright spot detection was used on the deconvolved DAPI signal to identify individual nuclei and automated DAPI channel thresholding was used to select the ONL. An automated GFP channel threshold calculated from the nonspecific GFP signal in the ONL in each image was used to define GFP-positive pixels. All ONL nuclei were then classified as GFP-positive or GFP-negative depending on present or absent overlap of their centroids with GFP-positive pixels. All analysis steps were deployed automatically and applied identically to each image.

Histopathology and analysis

Hematoxylin and eosin staining was performed on 14- μ m cryosections by the Morphology Core at the Abigail Wexner Research Institute at Nationwide Children's Hospital. Data were sampled from at least $n = 3$ eyes per vector construct. Five retina cryosections were obtained from each eye. All sections were evaluated by a trained retinal surgeon for possible abnormal pathology or signs of inflammation. Two of five sections (30X Nikon Ti2-E brightfield stitched images) were used to measure INL and ONL thickness. Measurements were

taken from 15 locations spanning the entirety of the retina by using the measurement tool provided in the NIS-Elements AR Analysis software. Measurement locations were completely randomized. All statistical analysis was performed on GraphPad Prism (v 9.0.0, GraphPad Software). Results are reported as mean \pm the standard error of the mean (SEM). Differences in thickness between vector-treated retinas compared with the control were assessed using a one-way ANOVA with Dunnett's multiple comparisons test. Differences were regarded significant where the multiplicity adjusted p value was <0.05 .

Total anti-AAV IgG in human sera

Indirect ELISAs were performed using sera collected from 12 human subjects. This research adhered to the tenets of the Declaration of Helsinki. All participant subjects signed an informed consent allowing samples to be used for research purposes. Immulon 4HBX microtiter plates (Cat3855, Thermo Fisher Scientific) were coated with 1×10^9 vector particles per well of AAV1, AAV2, AAV8, AAV9, or Anc80 empty capsids. Serial dilutions of sera were performed from 1:50 to 1:51,200. Secondary antibodies were conjugated with peroxidase (rabbit anti-human IgG [whole molecule]-peroxidase; Sigma A8792, Sigma-Aldrich, St. Louis, MO). Detection was via 3, 3', 5, 5'-tetramethylbenzidine (TMB) substrate reagent (T0440-100M, Millipore Sigma). Absorbance was measured at 450 nm in a BioTek Synergy 2 reader (BioTek, Shoreline, WA). Samples with an OD450 ratio (mean of coated – mean of uncoated/mean of uncoated) less than 0.2 were considered negative and samples greater than or equal to 0.5 were considered positive at any given dilution. Samples negative at 1:50 were considered to be below the detection limit. Samples were run in duplicate.

Statistics

All statistical analysis was performed on GraphPad Prism (v 9.0.0, GraphPad Software). For retinal cell quantification, results are reported as mean \pm SEM. Differences in transduction between cell types per vector were assessed using a one-way ANOVA with Tukey's multiple comparisons test. Differences were regarded significant where the multiplicity adjusted p value was <0.05 . AI software counts were compared with initial hand counts (Figure S2) performed on GFP+/Sox2+ retinas from each treatment group ($n = 3$). Pearson's correlation coefficient was calculated to determine the goodness of fit between Nikon and hand counts. R^2 values closest to 1 indicate a strong, positive correlation, whereas R^2 values closer to 0 indicate weak, negative correlation.

DATA AVAILABILITY

All data generated or analyzed during this study are included in this published article (and its supplementary information files). Raw data can be made available from the corresponding author upon reasonable request under MTA.

SUPPLEMENTAL INFORMATION

Supplemental information can be found online at <https://doi.org/10.1016/j.omtm.2023.05.016>.

ACKNOWLEDGMENTS

We would like to especially thank Dr. Luk Vandenberghe for publicly providing the An80 capsid for vector generation. Thank you to SAB Tech Inc. for producing the vectors described in this study and their commitment to quality. Thank you to the Animal Resource Core at NCH for maintaining the high quality of care provided to our animals. This study was funded by internal funds of the Abigail Wexner Research Institute, Nationwide Children's Hospital.

AUTHOR CONTRIBUTIONS

M.S. designed experiments, gathered and analyzed data, constructed the figures, and wrote the manuscript. T.V. developed the retinal quantification protocol, analyzed data, and constructed figures. M.B. assisted in executing experiments and editing the manuscript. V.M. determined vector concentrations. A.S.D. provided human serum samples. S.L. provided intellectual guidance, designed experiments, analyzed data, and edited the manuscript. A.B. provided intellectual guidance and edited the manuscript. K.M. provided intellectual guidance, edited the manuscript, and provided funding for completion of this study.

DECLARATION OF INTERESTS

K.M. is receiving royalties from Gene Therapy programs licensed to Amicus Therapeutics and Kiadis. K.M. is a scientific advisor with compensation and stock options and has received research funding from Alcyone Therapeutics.

REFERENCES

- Au, H.K.E., Isalan, M., and Mielcarek, M. (2022). Gene therapy advances: a meta-analysis of AAV usage in clinical settings. *Front. Med.* 8, 2746. <https://doi.org/10.3389/FMED.2021.809118/BIBTEX>.
- Kuzmin, D.A., Shutova, M.V., Johnston, N.R., Smith, O.P., Fedorin, V.V., Kukushkin, Y.S., van der Loo, J.C.M., and Johnstone, E.C. (2021). The clinical landscape for AAV gene therapies. *Nat. Rev. Drug Discov.* 20, 173–174. <https://doi.org/10.1038/d41573-021-00017-7>.
- Mendell, J.R., Al-Zaidy, S.A., Rodino-Klapac, L.R., Goodspeed, K., Gray, S.J., Kay, C.N., Boye, S.L., Boye, S.E., George, L.A., Salabarria, S., et al. (2021). Current clinical applications of in vivo gene therapy with AAVs. *Mol. Ther.* 29, 464–488. <https://doi.org/10.1016/j.ymt.2020.12.007>.
- Fuller-Carter, P.I., Basiri, H., Harvey, A.R., and Carvalho, L.S. (2020). Focused update on AAV-based gene therapy clinical trials for inherited retinal degeneration. *BioDrugs* 34, 763–781. <https://doi.org/10.1007/S40259-020-00453-8>.
- Aslesh, T., and Yokota, T. (2022). Restoring SMN expression: an Overview of the therapeutic developments for the treatment of spinal muscular atrophy. *Cells* 11, 417. <https://doi.org/10.3390/CELLS11030417>.
- Mendell, J.R., Al-Zaidy, S., Shell, R., Arnold, W.D., Rodino-Klapac, L.R., Prior, T.W., Lowes, L., Alfano, L., Berry, K., Church, K., et al. (2017). Single-dose gene-replacement therapy for spinal muscular atrophy. *N. Engl. J. Med.* 377, 1713–1722. <https://doi.org/10.1056/NEJMoa1706198>.
- Dhurandhar, D., Sahoo, N.K., Mariappan, I., and Narayanan, R. (2021). Gene therapy in retinal diseases: a review. *Indian J. Ophthalmol.* 69, 2257–2265. https://doi.org/10.4103/IJO.IJO_3117_20.
- Ross, M., and Ofri, R. (2021). The future of retinal gene therapy: evolving from subretinal to intravitreal vector delivery. *Neural Regen. Res.* 16, 1751–1759. <https://doi.org/10.4103/1673-5374.306063>.
- Ladha, R., Caspers, L.E., Willerman, F., and de Smet, M.D. (2022). Subretinal therapy: technological solutions to surgical and immunological challenges. *Front. Med.* 9, 661. <https://doi.org/10.3389/FMED.2022.846782/BIBTEX>.
- Mcmenamin, P.G., Saban, D.R., Dando, S.J., and Mcmenamin, P.G. (2020). Immune cells in the retina and choroid: two different tissue environments that require different defenses and surveillance. *Prog. Retin. Eye Res.* 70, 85–98. <https://doi.org/10.1016/j.preteyeres.2018.12.002>.
- Reichel, F.F., Peters, T., Wilhelm, B., Biel, M., Ueffing, M., Wissinger, B., Bartz-Schmidt, K.U., Klein, R., Michalakos, S., and Fischer, M.D.; RD-CURE Consortium (2018). Humoral immune response after intravitreal but not after subretinal AAV8 in primates and patients. *Invest. Ophthalmol. Vis. Sci.* 59, 1910–1915. <https://doi.org/10.1167/IOVS.17-22494>.
- Bouquet, C., Vignal Clermont, C., Galy, A., Fitoussi, S., Blouin, L., Munk, M.R., Valero, S., Meunier, S., Katz, B., Sahel, J.A., et al. (2019). Immune response and intraocular inflammation in patients with leber hereditary optic neuropathy treated with intravitreal injection of recombinant adeno-associated virus 2 carrying the ND4 gene: a secondary analysis of a phase 1/2 clinical trial. *JAMA Ophthalmol.* 137, 399–406. <https://doi.org/10.1001/JAMAOPHTHALMOL.2018.6902>.
- Timmers, A.M., Newmark, J.A., Turunen, H.T., Farivar, T., Liu, J., Song, C., Ye, G.J., Pennock, S., Gaskin, C., Knop, D.R., et al. (2020). Ocular inflammatory response to intravitreal injection of adeno-associated virus vector: relative contribution of genome and capsid. *Hum. Gene Ther.* 31, 80–89. <https://doi.org/10.1089/hum.2019.144>.
- Anderson, W.J., da Cruz, N.F.S., Lima, L.H., Emerson, G.G., Rodrigues, E.B., and Melo, G.B. (2021). Mechanisms of sterile inflammation after intravitreal injection of antiangiogenic drugs: a narrative review. *Int. J. Retin. Vitre.* 7, 37. <https://doi.org/10.1186/S40942-021-00307-7/TABLES/2>.
- Grzybowski, A., Told, R., Sacu, S., Bandello, F., Moisseiev, E., Loewenstein, A., and Schmidt-Erfurth, U.; Euretina Board (2018). 2018 update on intravitreal injections: euretina expert consensus recommendations. *Ophthalmologica* 239, 181–193. <https://doi.org/10.1159/000486145>.
- Ghoraba, H.H., Akhavanrezayat, A., Karaca, I., Yavari, N., Lajevardi, S., Hwang, J., Regenold, J., Matsumiya, W., Pham, B., Zaidi, M., et al. (2022). Ocular gene therapy: a literature review with special focus on immune and inflammatory responses. *Clin. Ophthalmol.* 16, 1753–1771. <https://doi.org/10.2147/OPTH.S364200>.
- Reichel, F.F.L., Wozar, F., Seitz, I., Ochakovski, A., Bartz-Schmidt, K.U., Peters, T., and Fischer, M.D.; RD-CURE Consortium (2021). An optimized treatment protocol for subretinal injections limits intravitreal vector distribution. *Ophthalmol. Sci.* 1, 100050. <https://doi.org/10.1016/J.XOPS.2021.100050>.
- Dalkara, D., Kolstad, K.D., Caporale, N., Visel, M., Klimczak, R.R., Schaffer, D.V., and Flannery, J.G. (2009). Inner limiting membrane barriers to AAV-mediated retinal transduction from the vitreous. *Mol. Ther.* 17, 2096–2102. <https://doi.org/10.1038/mt.2009.181>.
- Takahashi, K., Igarashi, T., Miyake, K., Kobayashi, M., Yaguchi, C., Iijima, O., Yamazaki, Y., Katakai, Y., Miyake, N., Kameya, S., et al. (2017). Improved intravitreal AAV-mediated inner retinal gene transduction after surgical internal limiting membrane peeling in cynomolgus monkeys. *Mol. Ther.* 25, 296–302. <https://doi.org/10.1016/j.ymt.2016.10.008>.
- Cehajic-Kapetanovic, J., Milosavljevic, N., Bedford, R.A., Lucas, R.J., and Bishop, P.N. (2018). Efficacy and safety of glycosidic enzymes for improved gene delivery to the retina following intravitreal injection in mice. *Mol. Ther. Methods Clin. Dev.* 9, 192–202. <https://doi.org/10.1016/j.omtm.2017.12.002>.
- Yiu, G., Chung, S.H., Mollhoff, I.N., Nguyen, U.T., Thomasy, S.M., Yoo, J., Taraborelli, D., and Noronha, G. (2020). Suprachoroidal and subretinal injections of AAV using transscleral microneedles for retinal gene delivery in nonhuman primates. *Mol. Ther. Methods Clin. Dev.* 16, 179–191. <https://doi.org/10.1016/j.omtm.2020.01.002>.
- Lee, E.J., Guenther, C.M., and Suh, J. (2018). Adeno-associated virus (AAV) vectors: rational design strategies for capsid engineering. *Curr. Opin. Biomed. Eng.* 7, 58–63. <https://doi.org/10.1016/J.COBME.2018.09.004>.
- Bartel, M.A., Weinstein, J.R., and Schaffer, D.V. (2012). Directed evolution of novel adeno-associated viruses for therapeutic gene delivery. *Gene Ther.* 19, 694–700. <https://doi.org/10.1038/gt.2012.20>.
- Zinn, E., Pacouret, S., Khaychuk, V., Turunen, H.T., Carvalho, L.S., Andres-Mateos, E., Shah, S., Shelke, R., Maurer, A.C., Plovie, E., et al. (2015). In silico reconstruction of the viral evolutionary lineage yields a potent gene therapy vector. *Cell Rep.* 12, 1056–1068. <https://doi.org/10.1016/j.celrep.2015.07.019>.

25. Carvalho, L.S., Xiao, R., Wassmer, S.J., Langsdorf, A., Zinn, E., Pacouret, S., Shah, S., Comander, J.J., Kim, L.A., Lim, L., et al. (2018). Synthetic adeno-associated viral vector efficiently targets mouse and non-human primate retina in vivo. *Hum. Gene Ther.* 29, 771–784. <https://doi.org/10.1089/hum.2017.154>.
26. Drack, A., Mahoney, A.V., Bhattarai, S., Mayer, S., Thomas, J., Datta, P., Hsu, Y., Garrison, J., Heon, E., Searby, C., et al. (2021). Subretinal gene replacement rescues retinal phenotype in BBS10 mouse. *Investig. Ophthalmol. Vis. Sci.* 62, 1178. <https://iovs.arvojournals.org/article.aspx?articleid=2773557>.
27. Hudry, E., Andres-Mateos, E., Lerner, E.P., Volak, A., Cohen, O., Hyman, B.T., Maguire, C.A., and Vandenberghe, L.H. (2018). Efficient gene transfer to the central nervous system by single-stranded Anc80L65. *Mol. Ther. Methods Clin. Dev.* 10, 197–209. <https://doi.org/10.1016/j.omtm.2018.07.006>.
28. Ezra-Elia, R., Obolensky, A., Ejzenberg, A., Ross, M., Mintz, D., Banin, E., and Ofri, R. (2018). Can an in vivo imaging system be used to determine localization and bio-distribution of AAV5-mediated gene expression following subretinal and intravitreal delivery in mice? *Exp. Eye Res.* 176, 227–234. <https://doi.org/10.1016/j.exer.2018.08.021>.
29. Cukras, C., Wiley, H.E., Jeffrey, B.G., Sen, H.N., Turrieff, A., Zeng, Y., Vijayarath, C., Marangoni, D., Ziccardi, L., Kjellstrom, S., et al. (2018). Retinal AAV8-RS1 gene therapy for X-linked retinoschisis: initial findings from a phase I/IIa trial by intravitreal delivery. *Mol. Ther.* 26, 2282–2294. <https://doi.org/10.1016/j.ymt.2018.05.025>.
30. Duong, T.T., Lim, J., Vasireddy, V., Papp, T., Nguyen, H., Leo, L., Pan, J., Zhou, S., Chen, H.I., Bennett, J., et al. (2019). Comparative AAV-EGFP transgene expression using vector serotypes 1–9, 7M8, and 8b in human pluripotent stem cells, RPEs, and human and rat cortical neurons. *Stem Cells Int.* 2019, 7281912. <https://doi.org/10.1155/2019/7281912>.
31. Pang, J.J., Lauramore, A., Deng, W.t., Li, Q., Doyle, T.J., Chiodo, V., Li, J., and Hauswirth, W.W. (2008). Comparative analysis of in vivo and in vitro AAV vector transduction in the neonatal mouse retina: effects of serotype and site of administration. *Vis. Res.* 48, 377–385. <https://doi.org/10.1016/j.visres.2007.08.009>.
32. Lee, S.H., Yang, J.Y., Madrakhimov, S., Park, H.Y., Park, K., and Park, T.K. (2019). Adeno-associated viral vector 2 and 9 transduction is enhanced in streptozotocin-induced diabetic mouse retina. *Mol. Ther. Methods Clin. Dev.* 13, 55–66. <https://doi.org/10.1016/j.omtm.2018.11.008>.
33. Murray, S.J., Russell, K.N., Melzer, T.R., Gray, S.J., Heap, S.J., Palmer, D.N., and Mitchell, N.L. (2021). Intravitreal gene therapy protects against retinal dysfunction and degeneration in sheep with CLN5 Batten disease. *Exp. Eye Res.* 207, 108600. <https://doi.org/10.1016/j.exer.2021.108600>.
34. Johnson, T.B., White, K.A., Brudvig, J.J., Cain, J.T., Langin, L., Pratt, M.A., Booth, C.D., Timm, D.J., Davis, S.S., Meyerink, B., et al. (2021). AAV9 gene therapy increases lifespan and treats pathological and behavioral abnormalities in a mouse model of CLN8-batten disease. *Mol. Ther.* 29, 162–175. <https://doi.org/10.1016/j.ymt.2020.09.033>.
35. Bosch, M.E., Aldrich, A., Fallet, R., Odvody, J., Burkovetskaya, M., Schuberth, K., Fitzgerald, J.A., Foust, K.D., and Kielian, T. (2016). Self-complementary AAV9 gene delivery partially corrects pathology associated with juvenile neuronal ceroid lipofuscinosis (CLN3). *J. Neurosci.* 36, 9669–9682. <https://doi.org/10.1523/JNEUROSCI.1635-16.2016>.
36. Day, T.P., Byrne, L.C., Schaffer, D.V., and Flannery, J.G. (2014). Advances in AAV vector development for gene therapy in the retina. *Adv. Exp. Med. Biol.* 801, 687–693. https://doi.org/10.1007/978-1-4614-3209-8_86.
37. Domenger, C., and Grimm, D. (2019). Next-generation AAV vectors—do not judge a virus (only) by its cover. *Hum. Mol. Genet.* 28, R3–R14. <https://doi.org/10.1093/HMG/DDZ148>.
38. Grimm, D., and Büning, H. (2017). Small but increasingly mighty: latest advances in AAV vector research, design, and evolution. *Hum. Gene Ther.* 28, 1075–1086. <https://doi.org/10.1089/HUM.2017.172>.
39. Tse, L.V., Moller-Tank, S., and Asokan, A. (2015). Strategies to circumvent humoral immunity to adeno-Associated viral vectors. *Expert Opin. Biol. Ther.* 15, 845–855. <https://doi.org/10.1517/14712598.2015.1035645>.
40. Kaiser, R.A., Weber, N.D., Trigueros-Motos, L., Allen, K.L., Martinez, M., Cao, W., VanLith, C.J., Hillin, L.G., Douar, A., González-Aseguinolaza, G., et al. (2021). Use of an adeno-associated virus serotype Anc80 to provide durable cure of phenylketonuria in a mouse model. *J. Inher. Metab. Dis.* 44, 1369–1381. <https://doi.org/10.1002/JIMD.12392>.
41. Pan, B., Askew, C., Galvin, A., Heman-Ackah, S., Asai, Y., Indzhykulia, A.A., Jodelka, F.M., Hastings, M.L., Lentz, J.J., Vandenberghe, L.H., et al. (2017). Gene therapy restores auditory and vestibular function in a mouse model of usher syndrome type 1c. *Nat. Biotechnol.* 35, 264–272. <https://doi.org/10.1038/NBT.3801>.
42. Ikeda, Y., Sun, Z., Ru, X., Vandenberghe, L.H., and Humphreys, B.D. (2018). Efficient gene transfer to kidney mesenchymal cells using a synthetic adeno-associated viral vector. *J. Am. Soc. Nephrol.* 29, 2287–2297. <https://doi.org/10.1681/ASN.2018040426/DCSUPPLEMENTAL>.
43. Suzuki, J., Hashimoto, K., Xiao, R., Vandenberghe, L.H., and Liberman, M.C. (2017). Cochlear gene therapy with ancestral AAV in adult mice: complete transduction of inner hair cells without cochlear dysfunction. *Sci. Rep.* 7, 45524. <https://doi.org/10.1038/srep45524>.
44. Landegger, L.D., Pan, B., Askew, C., Wassmer, S.J., Gluck, S.D., Galvin, A., Taylor, R., Forge, A., Stankovic, K.M., Holt, J.R., et al. (2017). A synthetic AAV vector enables safe and efficient gene transfer to the mammalian inner ear. *Nat. Biotechnol.* 35, 280–284. <https://doi.org/10.1038/NBT.3781>.
45. Waldrop, M.A., Karingada, C., Storey, M.A., Powers, B., Iammarino, M.A., Miller, N.F., Alfano, L.N., Noritz, G., Rossman, I., Ginsberg, M., et al. (2020). Gene therapy for spinal muscular atrophy: safety and early outcomes. *Pediatrics* 146, e20200729. <https://doi.org/10.1542/PEDS.2020-0729>.
46. Cain, J.T., Likhite, S., White, K.A., Timm, D.J., Davis, S.S., Johnson, T.B., Dennys-Rivers, C.N., Rinaldi, F., Motti, D., Corcoran, S., et al. (2019). Gene therapy corrects brain and behavioral pathologies in CLN6-batten disease. *Mol. Ther.* 27, 1836–1847. <https://doi.org/10.1016/j.ymt.2019.06.015>.
47. Vandenberghe, L.H., Bell, P., Maguire, A.M., Xiao, R., Hopkins, T.B., Grant, R., Bennett, J., and Wilson, J.M. (2013). AAV9 targets cone photoreceptors in the nonhuman primate retina. *PLoS One* 8, e53463. <https://doi.org/10.1371/journal.pone.0053463>.
48. McCarty, D.M. (2008). Self-complementary AAV vectors; advances and applications. *Mol. Ther.* 16, 1648–1656. <https://doi.org/10.1038/MT.2008.171>.
49. Xiong, W., Wu, D.M., Xue, Y., Wang, S.K., Chung, M.J., Ji, X., Rana, P., Zhao, S.R., Mai, S., and Cepko, C.L. (2019). AAV cis-regulatory sequences are correlated with ocular toxicity. *Proc. Natl. Acad. Sci. USA* 116, 5785–5794. <https://doi.org/10.1073/pnas.1821000116>.
50. Shen, J., Wang, Y., and Yao, K. (2021). Protection of retinal ganglion cells in glaucoma: current status and future. *Exp. Eye Res.* 205, 108506. <https://doi.org/10.1016/j.exer.2021.108506>.
51. Scalabrino, M.L., Boye, S.L., Fransen, K.M.H., Noel, J.M., Dyka, F.M., Min, S.H., Ruan, Q., De Leeuw, C.N., Simpson, E.M., Gregg, R.G., et al. (2015). Intravitreal delivery of a novel AAV vector targets ON bipolar cells and restores visual function in a mouse model of complete congenital stationary night blindness. *Hum. Mol. Genet.* 24, 6229–6239. <https://doi.org/10.1093/hmg/ddv341>.
52. Kleine Holthaus, S.M., Aristorena, M., Maswood, R., Semenyuk, O., Hoke, J., Hare, A., Smith, A.J., Mole, S.E., and Ali, R.R. (2020). Gene therapy targeting the inner retina rescues the retinal phenotype in a mouse model of CLN3 batten disease. *Hum. Gene Ther.* 31, 709–718. <https://doi.org/10.1089/hum.2020.038>.
53. kleine Holthaus, S.M., Ribeiro, J., Abelleira-Hervas, L., Pearson, R.A., Duran, Y., Georgiadis, A., Sampson, R.D., Rizzi, M., Hoke, J., Maswood, R., et al. (2018). Prevention of photoreceptor cell loss in a CLN6 mouse model of batten disease requires CLN6 gene transfer to bipolar cells. *Mol. Ther.* 26, 1343–1353. <https://doi.org/10.1016/j.ymt.2018.02.027>.
54. Bringmann, A., and Wiedemann, P. (2012). Müller glial cells in retinal disease. *Ophthalmologica* 227, 1–19. <https://doi.org/10.1159/000328979>.
55. Bringmann, A., Pannicke, T., Grosche, J., Francke, M., Wiedemann, P., Skatchkov, S.N., Osborne, N.N., and Reichenbach, A. (2006). Müller cells in the healthy and diseased retina. *Prog. Retin. Eye Res.* 25, 397–424. <https://doi.org/10.1016/j.preteyeres.2006.05.003>.
56. Zhang, K.Y., and Johnson, T.V. (2021). The internal limiting membrane: roles in retinal development and implications for emerging ocular therapies. *Exp. Eye Res.* 206, 108545. <https://doi.org/10.1016/j.exer.2021.108545>.

57. Giove, T.J., Khankhel, Z.S., Sena-Esteves, M., and Eldred, W.D. (2009). Cellular tropism of Aav8, Aav9 and Aav10 in mouse retina. *Investig. Ophthalmol. Vis. Sci.* 50, 3013. <https://iovs.arvojournals.org/article.aspx?articleid=2365407>.
58. Mysore, N., Koenekoop, J., Li, S., Ren, H., Keser, V., Lopez-Solache, I., and Koenekoop, R.K. (2014). A review of secondary photoreceptor degenerations in systemic disease. *Cold Spring Harb. Perspect. Med.* 5, a025825. <https://doi.org/10.1101/CSHPERSPECT.A025825>.
59. Del Longo, A., Piozzi, E., and Schweizer, F. (2018). Ocular features in mucopolysaccharidosis: diagnosis and treatment 11 medical and health sciences 1113 ophthalmology and optometry. *Ital. J. Pediatr.* 44, 91–98. <https://doi.org/10.1186/S13052-018-0559-9/FIGURES/3>.
60. McClements, M.E., Staurengi, F., MacLaren, R.E., and Cehajic-Kapetanovic, J. (2020). Optogenetic gene therapy for the degenerate retina: recent advances. *Front. Neurosci.* 14, 1187. <https://doi.org/10.3389/FNINS.2020.570909/BIBTEX>.
61. Thwaite, R., Pagès, G., Chillón, M., and Bosch, A. (2015). AAVrh.10 immunogenicity in mice and humans. Relevance of antibody cross-reactivity in human gene therapy. *Gene Ther.* 22, 196–201. <https://doi.org/10.1038/GT.2014.103>.
62. Kotterman, M.A., Yin, L., Strazzeri, J.M., Flannery, J.G., Merigan, W.H., and Schaffer, D.V. (2015). Antibody neutralization poses a barrier to intravitreal adeno-associated viral vector gene delivery to non-human primates. *Gene Ther.* 22, 116–126. <https://doi.org/10.1038/gt.2014.115>.
63. Ail, D., Ren, D., Brazhnikova, E., Nouvel-Jaillard, C., Bertin, S., Mirashrafi, S.B., Fisson, S., and Dalkara, D. (2022). Systemic and local immune responses to intraocular AAV vector administration in non-human primates. *Mol. Ther. Methods Clin. Dev.* 24, 306–316. <https://doi.org/10.1016/J.OMTM.2022.01.011>.
64. Zhou, R., and Caspi, R.R. (2010). Ocular immune privilege Introduction and context. *F1000 Biol. Rep.* 2, 3. <https://doi.org/10.3410/B2-3>.
65. Chan, Y.K., Dick, A.D., Hall, S.M., Langmann, T., Scribner, C.L., and Mansfield, B.C.; Ocular Gene Therapy Inflammation Working Group (2021). Inflammation in viral vector-mediated ocular gene therapy: a review and report from a workshop hosted by the foundation fighting blindness, 9/2020. *Transl. Vis. Sci. Technol.* 10, 3. <https://doi.org/10.1167/TVST.10.4.3>.
66. Mendell, J.R., Connolly, A.M., Lehman, K.J., Griffin, D.A., Khan, S.Z., Dharia, S.D., Quintana-Gallardo, L., and Rodino-Klapac, L.R. (2022). Testing preexisting antibodies prior to AAV gene transfer therapy: rationale, lessons and future considerations. *Mol. Ther. Methods Clin. Dev.* 25, 74–83. <https://doi.org/10.1016/J.OMTM.2022.02.011>.
67. del Amo, E.M., Rimpelä, A.K., Heikkinen, E., Kari, O.K., Ramsay, E., Lajunen, T., Schmitt, M., Pelkonen, L., Bhattacharya, M., Richardson, D., et al. (2017). Pharmacokinetic aspects of retinal drug delivery. *Prog. Retin. Eye Res.* 57, 134–185. <https://doi.org/10.1016/J.PRETEYERES.2016.12.001>.
68. Tshilenge, K.T., Ameline, B., Weber, M., Mendes-Madeira, A., Nedellec, S., Biget, M., Provost, N., Libeau, L., Blouin, V., Deschamps, J.Y., et al. (2016). Vitrectomy before intravitreal injection of AAV2/2 vector promotes efficient transduction of retinal ganglion cells in dogs and nonhuman primates. *Hum. Gene Ther. Methods* 27, 122–134. <https://doi.org/10.1089/HGTB.2016.034>. <https://home.liebertpub.com/hgtb>.
69. Meyer, K., Ferraiuolo, L., Schmelzer, L., Braun, L., McGovern, V., Likhite, S., Michels, O., Govoni, A., Fitzgerald, J., Morales, P., et al. (2015). Improving single injection CSF delivery of AAV9-mediated gene therapy for SMA: a dose-response study in mice and nonhuman primates. *Mol. Ther.* 23, 477–487. <https://doi.org/10.1038/mt.2014.210>.
70. Foust, K.D., Wang, X., McGovern, V.L., Braun, L., Bevan, A.K., Haidet, A.M., Le, T.T., Morales, P.R., Rich, M.M., Burghes, A.H.M., et al. (2010). Rescue of the spinal muscular atrophy phenotype in a mouse model by early postnatal delivery of SMN. *Nat. Biotechnol.* 28, 271–274. <https://doi.org/10.1038/nbt.1610>.
71. Lock, M., Alvira, M.R., Chen, S.J., and Wilson, J.M. (2014). Absolute determination of single-stranded and self-complementary adeno-associated viral vector genome titers by droplet digital PCR. *Hum. Gene Ther. Methods* 25, 115–125. <https://doi.org/10.1089/HGTB.2013.131>.